Journal of Magnetism and Magnetic Materials 446 (2018) 239–244

Contents lists available at ScienceDirect

Journal of Magnetism and Magnetic Materials

journal homepage: www.elsevier.com/locate/jmmm

Research articles

Separating the influence of electric charges in magnetic force microscopy images of inhomogeneous metal samples

Mónica P. Arenas [a,b,*], Evandro M. Lanzoni [c,d], Clara J. Pacheco [b], Carlos A.R. Costa [c], Carlos B. Eckstein [e], Luiz H. de Almeida [a], João M.A. Rebello [a], Christoph F. Deneke [f], Gabriela R. Pereira [a,b]

[a] Department of Metallurgical and Materials Engineering – UFRJ, Rio de Janeiro, RJ 21941-972, Brazil
[b] Laboratory of Nondestructive Testing, Corrosion and Welding, Rio de Janeiro, RJ 21941-596, Brazil
[c] Brazilian Nanotechnology National Laboratory, Campinas, SP 18083-970, Brazil
[d] São Paulo State University – UNESP, Sorocaba, SP 18087-180, Brazil
[e] Petrobras, Rio de Janeiro, RJ 21040-000, Brazil
[f] Gleb Wataghin Institute of Physics, University of Campinas, SP 13083859, Brazil

ARTICLE INFO

Article history:
Received 3 July 2017
Received in revised form 11 September 2017
Accepted 17 September 2017
Available online 19 September 2017

Keywords:
Austenitic stainless steels
Aging
Carbides
Magnetic force microscopy
Kelvin probe force microscopy
Magnetic properties

ABSTRACT

In this study, we investigate artifacts arising from electric charges present in magnetic force microscopy images. Therefore, we use two austenitic steel samples with different microstructural conditions. Furthermore, we examine the influence of the surface preparation, like etching, in magnetic force images. Using Kelvin probe force microscopy we can quantify the charges present on the surface. Our results show that electrical charges give rise to a signature in the magnetic force microscopy, which is indistinguishable from a magnetic signal. Our results on two differently aged steel samples demonstrate that the magnetic force microscopy images need to be interpreted with care and must be corrected due to the influence of electrical charges present. We discuss three approaches, how to identify these artifacts – parallel acquisition of magnetic force and electric force images on the same position, sample surface preparation to decrease the presence of charges and inversion of the magnetic polarization in two succeeding measurement.

1. Introduction

Magnetic force microscopy [1–4] (MFM) is one of the oldest modification of the atomic force microscope [5] used to investigate the magnetic domain structure of various materials. This well-established technique is able to image the magnetic signature of a sample by scanning a magnetic tip in some distance over the surface achieving a lateral resolution of ca. 20 nm [3]. In contrast to electric force microscopy (EFM) or the related method of Kelvin probe force microscopy (KPFM) [6–8], only a qualitative description of the forces are possible as the exact tip-sample interaction is hard to model [4]. In recent years, MFM moved from imaging strong magnetic fields e.g. in storage devices [3] to the detection of weak magnetic signatures e.g. magnetic moments from polymer radicals [9,10]. It has been pointed out [11] that for such weak magnetic signals, the force by present electric charges or electrical surface potential can be in the same order of magnitude or higher. Furthermore, a compensation scheme was suggested to suppress the influence of such electric potentials resulting from the work function difference of dissimilar materials [11]. A separation of electrical and magnetic signals is especially important for materials with phase separations like metal alloys with precipitations such as certain stainless steels, but rarely implemented in praxis.

Centrifugally cast modified-HP heat-resistant austenitic stainless steels exhibit mechanical properties enabling them to withstand harsh operational conditions such as high temperatures and pressures [12]. They are commonly used as radiant tubes in pyrolysis and reformer furnaces [13,14]. In reforming, endothermic reactions take place inside vertical catalyst-filled tubes, which feed into a collector header. The skin temperatures of these tubes are usually in the range of 600–1000 °C and the tubes experience internal pressures up to 4 MPa [13,15]. During aging, the as-cast microstructure exhibits changes such as the coarsening of primary eutectic carbides, fine secondary precipitation of Cr carbides, and

* Corresponding author at: Department of Metallurgical and Materials Engineering – UFRJ, Rio de Janeiro, RJ 21941-972, Brazil.
E-mail addresses: monica.correa@metalmat.ufrj.br (M.P. Arenas), evandro.lanzoni@lnnano.cnpem.br (E.M. Lanzoni), cjpacheco@metalmat.ufrj.br (C.J. Pacheco), carlos.costa@lnnano.cnpem.br (C.A.R. Costa), brunoeck@petrobras.com.br (C.B. Eckstein), lha@metalmat.ufrj.br (L.H. de Almeida), jmarcos@metalmat.ufrj.br (J.M.A. Rebello), cdeneke@ifi.unicamp.br (C.F. Deneke), gpereira@metalmat.ufrj.br (G.R. Pereira).

https://doi.org/10.1016/j.jmmm.2017.09.041
0304-8853/

in situ transformation of NbC in the G-phase ($Ni_{16}Nb_6Si_7$) [16,17]. These microstructural transformations cause variations in magnetic and electrical properties [18].

Recently, MFM, EFM and KPFM have been used to characterize the ferrite, austenite, and other phases in a duplex stainless steel (DSS) [19,20]. The combination of both techniques proved to be a powerful tool to distinguish ferrite from austenite phases with high spatial resolution [19,21–23]. However, this does not include studies correlating the state of aging of an austenitic HP steel with its magnetic and electrical properties. Furthermore, the influence of the present electrical charges – e.g. in non-magnetic and non-metallic precipitations like carbides – to MFM measurements need to be investigated to correctly interpret results obtained on such inhomogeneous samples.

In this work, we analyze the transition of electric potential difference and magnetic properties using MFM, EFM and KPFM of a modified-HP samples with two different states of aging. We show that the occurrence of the different phases in these steels require care in the data interpretation. We demonstrate that the magnetic signal deducted in MFM is cross-contaminated by an EFM signal arising from the difference of the work function or electric charges present in carbides in the austenitic matrix. We quantify the present charges by KPFM and demonstrate the introduction of charges (and their removal) by commonly used sample preparation process of the steel samples. Furthermore, we can separate the magnetic contribution from the electrical contribution by polarization inversion of the magnetic domains of the steel. Our results on two differently aged steel samples demonstrate that the combination of MFM images of inhomogeneous samples are need to be interpreted with care and most be corrected due to the influence of electrical charges present.

2. Experiments

2.1. Samples

For better understanding, we discuss the expected microstructure for different life time and temperatures – normally given in aging stages I–VI – for the samples. The as-cast condition and aging state I microstructure is composed of an austenitic matrix with an interdendritic primary network of chromium carbide ($Cr_{23}C_6$) and niobium-titanium carbide (NbTi-C) [24,25]. Once the modified HP-NbTi steel is exposed to temperatures between 600 °C and 800 °C, a fine distribution of Cr secondary carbides is dispersed in the austenitic matrix, which is distributed adjacent to the primary carbide network [14]. These temperatures cause aging states II or III. Once the alloy is exposed to temperatures between 800 °C and 1000 °C, it may exhibit aging states between IV and VI [12,14]. The microstructures of these stages include larger, coalesced secondary chromium carbides in the intradendritic region and (Nb, Ti)C is partially transformed into the G-phase [25–27]. This transformation also depends on the silicon and niobium content [17,28].

Our two investigated samples were taken from a modified HP-NbTi tube removed from service after 90,000 h. The two samples were taken from two different regions of the steam reformer tube exposed to 600 °C and 1000 °C, respectively. Hence, the samples exhibited aging states I and VI, respectively. The samples were extracted from the cross-section of the tubes (10 mm × 13 mm × 5 mm). To improve the surface finishing, the samples were sanded with 1500-grit sandpaper and polished using 1 μm diameter diamond paste.

Backscattering scanning electron microscopy (BSE) was carried out for microstructural characterization in order to identify different phases using their atomic weights allowing to differentiate between Cr and Nb,Ti carbides.

In order to observe the influence of the surface finishing on MFM, EFM and KPFM, the measurements were performed on samples with and without chemical etching. The etching was carried out for two seconds with 63% H_3PO_4:15% H_2SO_4:22% H_2O solution. After the surface finishing, the bulk was marked to image the same region by MFM, EFM and KPFM.

X-ray fluorescence technique was deducted on the sample with aging I for the chemical analysis, as shown in Table 1. The concentrations of all chemical elements are within the ASTM A297 standard [29], except for niobium and titanium, indicating that is a modified HP-Nb, microalloyed with Ti.

2.2. SPM techniques

MFM, EFM and KPFM were executed using a FlexAFM (Nanosurf AG, Liestal, Switzerland) of the LNNano/CNPEM facilities. All measurements were conducted in air at room temperature. A cobalt-coated silicon probe (PPP-MFM Nanosensors) was used for MFM. The used probes exhibit a resonant frequency (f) and force constant (k) i.e. f = 75 kHz and k = 2.8 Nm^{-1}.

The MFM data is acquired in two steps (double pass). Therefore, the MFM tip is magnetized using a neodymium magnet (0.46 T of remanent magnetization) prior to the measurements. The hard-magnetic cobalt will keep this initial magnetization and orientation throughout the MFM experiments. Initially, the topography of the sample is measured in intermittent contact mode. Then, the probe is lifted to a constant distance of 120 nm above the sample surface (lift mode), where magnetic forces are dominant. At this point, the phase-shift induced by the magnetic force gradient between the probe and the sample is acquired [1].

In order to distinguish the electrical from the magnetic signals, all MFM measurements were carried out in the presence of an external magnetic field from a permanent magnet. Therefore, a permanent magnet was placed below the sample to control the orientation of the magnetic domains of the samples. Hereby, the relation between the tip magnetization and the sample magnetization can be tuned. As depicted in Fig. 1a, we acquire first images with sample and tip magnetization contrary. In a second set of measurements, magnetization of the sample is reversed, as shown in Fig. 1b. Hence, we expect an inversion of the magnetic signal in the MFM measurements, but electrical contribution will stay unchanged as the electrical force is not influenced by the external magnetic field.

Both EFM and KPFM techniques measure the electric force between the probe and the sample surface. EFM measures a qualitative (phase-shift) surface potential difference in lift mode [30], whereas KPFM maps show a quantitative electric potential difference on the surface. Indeed, EFM follows the acquisition scheme of MFM changing only the used tip. For EFM, a silicon probe coated with platinum-iridium (PPP-EFM Nanosensors) with same tip mechanical properties as the Co-coated MFM probes. KPFM was executed with Co coated MFM probes.

Table 1
Chemical composition of the modified HP stainless steel alloy. Composition balanced by %Fe.

	Cr	Ni	C	Mn	Si	P	S	Mo	Nb	Ti
wt%	25.5	35.0	0.54	1.3	1.6	0.02	0.006	0.01	1.13	0.083

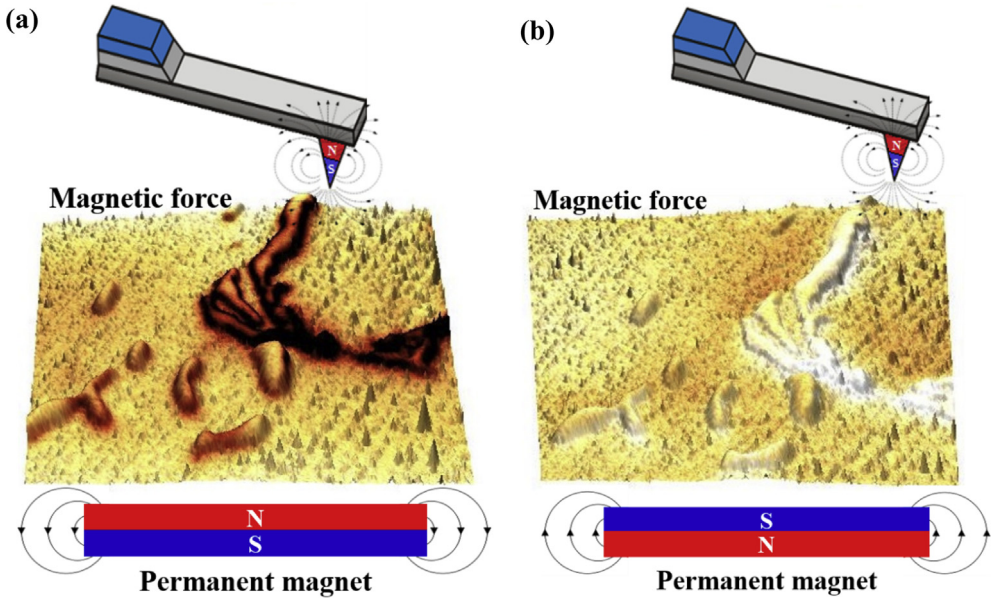

Fig. 1. MFM image overlaid with the topographic image showing the inversion of the contrast when changing the magnetic polarization of the permanent magnet placed below the sample. MFM image (a) in attractive mode and (b) repulsive mode between the probe and sample.

The KPFM measurements are implemented in intermittent contact mode. The mechanical oscillation of the probe is tracked by a photodetector and analyzed using two feedback loops. The first loop is used in the conventional manner to control the probe-sample distance. The second loop is used to minimize the electric field between the probe and sample by adjusting the probe bias voltage [31]. Therefore, an electrical AC signal is applied to the probe at 15 kHz during image acquisition. A lock-in amplifier is used to measure the probe vibration at this frequency and a DC bias applied to minimize the signal at this oscillation frequency. The DC signal is used to build the KPFM image at each pixel, detecting electric potential throughout the scanned surface area allowing formation of the topographic and KPFM image in a single pass mode.

3. Results and discussion

3.1. MFM vs EFM signals

In order to show the influence of electrical charges and potential in an inhomogeneous material, we acquire MFM and EFM images in the same sample region of the stage I aged stainless steel sample. Hereby, we expect that the MFM, as it uses metallic/magnetic probe, will be sensitive to any magnetic as well as electrical signal present. In contrast, EFM should only detect electrical contributions. A comparison of the MFM and EFM images should allow separations of the two signals.

Fig. 2a depicts the AFM topographic image. We observe a small height contrast in the middle of the image. During surface preparation and final polishing, the harder carbide will be less sensitive to the mechanical polishing resulting in a slight elevation over the surrounding austenitic matrix. Fig. 2b shows an MFM image acquired with the Co coated probe allowing to identifying the carbide inside the austenite matrix. The region between the austenitic matrix (bright) and the interior of the carbide (dark) exhibits a strong contrast ascribed to a magnetic signal. The same region imaged by EFM using a Pt coated probe is seen in Fig. 2c. The magnetic signal of the carbide boundary disappears, but the carbide as whole still exhibits a clear contrast. Therefore, we ascribe the dark contrast at the carbide boundary to a magnetic signal. We attributed the presence of a magnetic phase to a localized chromium depletion around the carbides changing the austenitic to a magnetic ferritic phase [32–34].

It is worth pointing out that Fig. 2b and c images are highly correlated. Only the magnetic signal attributed to the carbide grain boundary disappears indicating that the contrast observed in the austenitic matrix and inside the carbide is due to the electrical

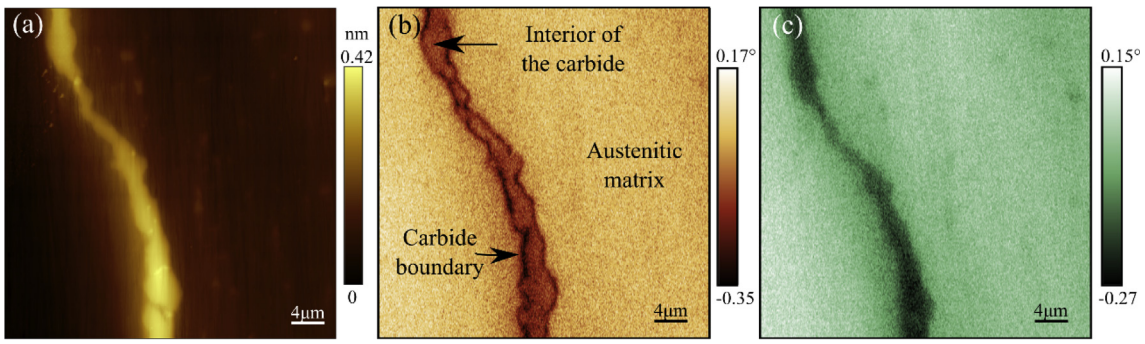

Fig. 2. Non-etched state I aged steel sample. (a) AFM surface topography, (b) MFM image of depicting the phase-shift using a typical MFM probe, (c) EFM phase-shift image obtained using an EFM probe. In MFM and EFM images, the contrast observed inside the carbide arises from the electric potential of the sample and only the contrast on the grain boundary is a true magnetic signature.

potential difference. Therefore, our first measurements demonstrate that the MFM images contain a large contribution due to electric charges on the sample surfaces, which are indistinguishable from the magnetic signature.

3.2. Artifact suppression by sample preparation

To observe the influence of surface finishing, samples of aging state VI steel were analyzed with MFM and KPFM with and without chemical etching. The measurements were completed in the presence of an external magnetic field in attractive mode. Fig. 3a–c depict the AFM topography, MFM and KPFM images from a non-etched sample surface at the same position, respectively. The topographic image in Fig. 3a allows to identify the austenitic matrix as well as the carbide. The MFM image (Fig. 3b) exhibits a weak contrast between the carbide precipitates and the austenitic matrix, similar to the one observed in Fig. 2b. The KPFM image (Fig. 3c) demonstrates a clear difference between the carbides and the austenitic matrix associating the dark regions in the KPFM image with carbides and the bright regions with the austenitic matrix. We estimate the contact potential difference between the carbide and the matrix to 60 mV.

Fig. 3d,f show the AFM topography, MFM and KPFM images obtained from a sample after chemical etching, respectively. We observed a clear topography contrast in Fig. 3d, but hardly any MFM contrast in Fig. 3e. This proofs that our MFM measurements are normally free from topography artifacts and signals seen arise either from magnetic or electrical forces present in the sample surface. Furthermore, the KPFM (Fig. 3f) image indicates now a contact potential difference of 12 mV between a carbide and the surrounding austenitic matrix. It has been previously reported that the contact difference potential in DSS samples is affected by etching or corrosion [19,20]. On the one hand, the KPFM indicates chemical etching tends to reduce the electric potential difference between the phases. On the other hand, the weak presents of a contrast in the MFM image – especially the clear decrease after etching – confirms our previous point that the presents of any electrical potential or charges give rise to artifacts in MFM images and a surface treatment decreasing the presence of charges significantly reducing such artifacts as demonstrated by our results.

3.3. Separating magnetic and electric signals by inversion of the magnetic domains

An elegant way to identify the magnetic domains of the sample and separate them from any electrical artifacts in the MFM images is taking advantage of the intrinsic difference between a magnetic and an electric force detected on scanning probe microscopy. Whereas the electric forces depend on the charges involved and are not influenced by external static magnetic fields, magnetic forces arising from magnetic domains of the sample can be inverted by an external magnetic field inverting these domains. Hence, reversing the direction of an external magnetic field reversing the magnetic domains but leaving the magnetization of the MFM probe unchanged, a contrast inversion in the MFM image can be achieved as lined out before.

Fig. 4a shows a SEM micrograph (backscatter mode) of the chemically etched sample of an aging state I steel. From the image, we conclude that the microstructure is composed of an austenitic matrix surrounded by chromium carbide (dark) and niobium-titanium carbide (bright). The carbide precipitates correlate well with the shapes ascribed to them in the AFM images. Fig. 4.b depicts the MFM phase-shift for one direction of the external field. The boundaries between the carbide and the austenitic matrix are dark due to the magnetic response. However, once the polarity of the permanent magnet is inverted, the magnetic forces between tip and sample also reverse giving rise to a contrast reversion as can observed in the MFM image depicted in Fig. 4c. For the inversed magnetic field, the boundaries between the austenitic matrix and the carbide are inverted in color, becoming bright. The boundaries of both the chromium and niobium-titanium carbides are well highlighted. Thus, we prove that the signal is a mag-

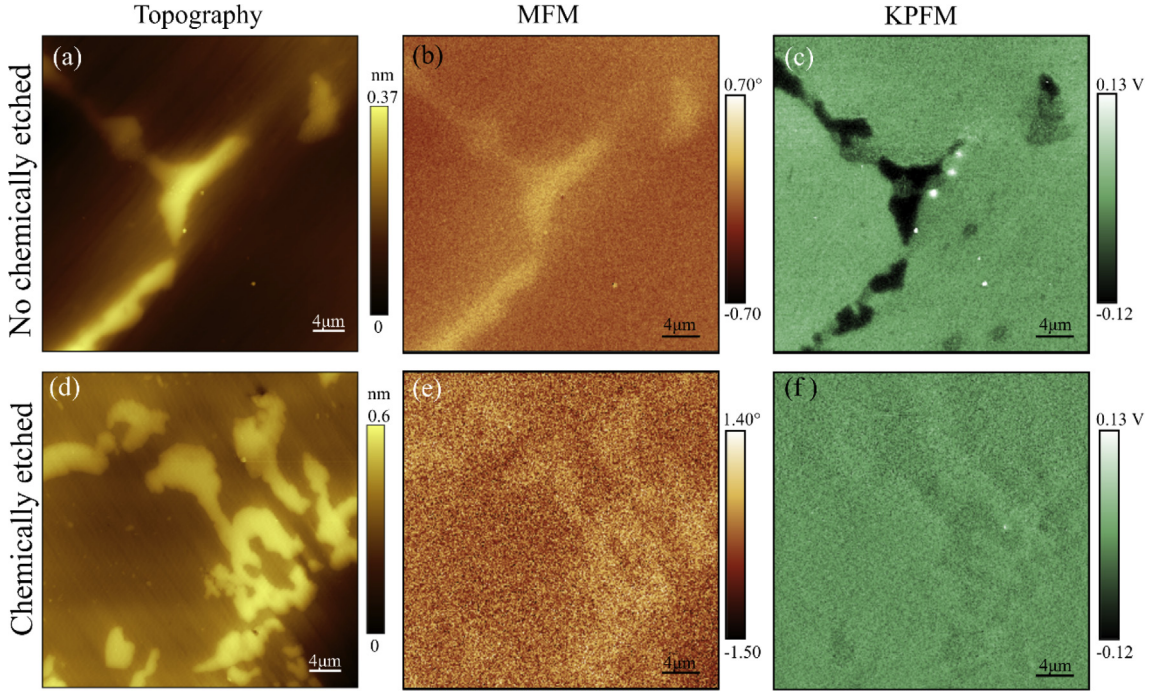

Fig. 3. Sample of an aged state VI steel before chemical etching (a) AFM surface topography, (b) MFM phase-shift image and (c) KPFM image. Same sample after chemical etching (d) AFM surface topography, (e) MFM phase-shift image and (f) KPFM image.

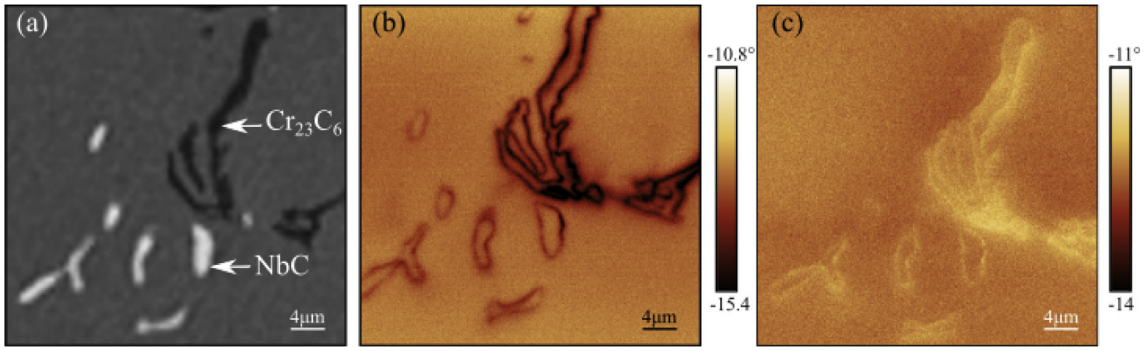

Fig. 4. Etched sample with aging state I: (a) SEM micrograph using backscattered electron mode, (b) MFM phase-shift image obtained with the magnet configured to attract the probe to the sample, (c) MFM phase-shift image measured with the magnet configured in repulsive mode.

netic signal and not an electrical artifact. The magnetic response arises only from the carbide boundaries, which we ascribe to the chromium depleted zone as previously discussed [32–34]. This depletion is sufficient to create a ferromagnetic ring around the carbides [32].

4. Conclusions

In summary, we demonstrated that for inhomogeneous samples, like modified-HP heat-resistant austenitic stainless steels, it is crucial to separate the influence of electrical charges from magnetic signatures in MFM images. We show that the sample preparation or the contact potential difference can give rise to false magnetic signatures in standard MFM measurements. We show three approaches to identify and separate such contributions: (i) by carrying out EFM on the same sample position, (ii) sample preparation that minimizes any charges in the sample (but artifacts may still be present due to contact potential differences) and finally (iii) by inverting the magnetic domains and thereby inverting the contrast of the MFM images. From the three discussed methods, (iii) seems the most promising one and superior to previously suggested electrical compensation schemes. Whereas any compensation requires the measurement and application of an external voltage that might introduce other artifacts, a magnetization of sample only requires a weak external field leaving the sample otherwise unchanged. Finally, we demonstrate that the carbides of our investigated steel samples of the aging state I have magnetic phase boundary towards the austenitic matrix, whereas other magnetic contrasts arise from present electric charges and fields.

Acknowledgments

The authors would like to thank Petrobras for providing samples and financial support, to Brazilian scientific funding agencies CAPES and CNPq, and LNNano/CNPEM (Brazil) for cooperation and assistance with experiments.

References

[1] Y. Martin, H.K. Wickramasinghe, Magnetic imaging by "force microscopy" 1000 with a resolution, Appl. Phys. Lett. 50 (1987) 1455–1457.
[2] J.J. Sáenz, N. García, P. Grütter, E. Meyer, H. Heinzelmann, R. Wiesendanger, L. Rosenthaler, H.R. Hidber, H.-J. Güntherodt, Observation of magnetic forces by the atomic force microscope, J. Appl. Phys. 62 (1987) 4293, https://doi.org/10.1063/1.339105.
[3] A. de Lozanne, Application of magnetic force microscopy in nanomaterials characterization, Microsc. Res. Tech. 69 (2006) 550–562, https://doi.org/10.1002/jemt.20325.
[4] U. Hartmann, Magnetic force microscopy, Annu. Rev. Mater. Sci. 29 (1999) 53, https://doi.org/10.1146/annurev.matsci.29.1.53.
[5] G. Binnig, C.F. Quate, C. Gerber, Atomic force microscope, Phys. Rev. Lett. 56 (1986) 930–933, https://doi.org/10.1103/PhysRevLett. 56.930.
[6] K.L. Sorokina, A.L. Tolstikhina, Atomic force microscopy modified for studying electric properties of thin films and crystals. Review, Crystallogr. Rep. 49 (2004) 476–499, https://doi.org/10.1134/1.1756648.
[7] W. Melitz, J. Shen, A.C. Kummel, S. Lee, Kelvin probe force microscopy and its application, Surf. Sci. Rep. 66 (2011) 1–27, https://doi.org/10.1016/j.surfrep.2010.10.001.
[8] P. Girard, Electrostatic force microscopy: principles and some applications to semiconductors, Nanotechnology 12 (2001) 485, https://doi.org/10.1088/0957-4484/12/4/321.
[9] M. Miyasaka, Y. Saito, H. Nishide, Magnetic force microscopy images of a nanometer-sized, purely organic high-spin polyradical, Adv. Funct. Mater. 13 (2003) 113–117, https://doi.org/10.1002/adfm.200390016.
[10] H.T. Baytekin, B. Baytekin, T.M. Hermans, B. Kowalczyk, B. Grzybowsk, Control of surface charges by radicals as a principle of antistatic polymers protecting electronic circuity, Science (80-.) 341 (2013) 1368–1371, https://doi.org/10.1126/science.1241326.
[11] M. Jaafar, O. Iglesias-Freire, L. Serrano-Ramón, M.R. Ibarra, J.M. de Teresa, A. Asenjo, Distinguishing magnetic and electrostatic interactions by a Kelvin probe force microscopy–magnetic force microscopy combination, Beilstein J. Nanotechnol. 2 (2011) 552–560, https://doi.org/10.3762/bjnano.2.59.
[12] T.L. da Silveira, I. Le May, Reformer furnaces: materials, damage mechanisms and assessment, Arab. J. Sci. Eng. 31 (2006) 99–119.
[13] E. Bullock, Developments in Heat-Resisting Alloys for Petrochemical Plant, in: Res. Dev. High Temp. Mater. Ind., Elsevier Applied Science, 1989, pp. 31–46.
[14] I. Le May, T.L. da Silveira, C.H. Vianna, Criteria for the evaluation of damage and remaining life in reformer furnace tubes, Int. J. Press. Vessels Pip. 66 (1996) 233–241.
[15] A. Alvino, D. Lega, F. Giacobbe, V. Mazzocchi, A. Rinaldi, Damage characterization in two reformer heater tubes after nearly 10 years of service at different operative and maintenance conditions, Eng. Fail. Anal. 17 (2010) 1526–1541.
[16] G.D. Barbabela, L.H. de Almeida, T.L. da Silveira, I. Le May, L.H. de Almeida, T.L. da Silveira, I. Le May, Phase characterization in two centrifugally cast HK stainless steel tubes, Mater. Charact. 26 (1991) 1–7.
[17] G.D. Barbabela, L.H. de Almeida, T.L. da Silveira, I. Le May, Role of Nb in modifying the microstructure of heat-resistant cast HP steel, Mater. Charact. 26 (1991) 193–197.
[18] J.M.B. Pereira, C.J. Pacheco, M.P. Arenas, J.F.D.F. Araujo, G.R. Pereira, A.C. Bruno, Novel scanning dc-susceptometer for characterization of heat-resistant steels with different states of aging, J. Magn. Magn. Mater. 442 (2017) 311–318, https://doi.org/10.1016/j.jmmm.2017.07.004.
[19] M. Femenia, C. Canalias, J. Pan, C. Leygraf, Scanning Kelvin probe force microscopy and magnetic force microscopy for characterization of duplex stainless steels, J. Electrochem. Soc. 150 (2003) B274–B281, https://doi.org/10.1149/1.1572482.
[20] J. Ramírez-Salgado, M.a. Domínguez-Aguilar, B. Castro-Domínguez, P. Hernández-Hernández, R.C. Newman, Detection of secondary phases in duplex stainless steel by magnetic force microscopy and scanning Kelvin probe force microscopy, Mater. Charact. 86 (2013) 250–262, https://doi.org/10.1016/j.matchar.2013.10.012.
[21] N. Sathirachinda, R. Pettersson, J. Pan, Depletion effects at phase boundaries in 2205 duplex stainless steel characterized with SKPFM and TEM/EDS, Corros. Sci. 51 (2009) 1850–1860.
[22] S. Wang, J. Ding, H. Ming, Z. Zhang, J. Wang, Characterization of low alloy ferritic steel – Ni base alloy dissimilar metal weld interface by SPM techniques, SEM/EDS, TEM/EDS and SVET, Mater. Charact. 100 (2015) 50–60.
[23] L.Q. Guo, M.C. Lin, L.J. Qiao, A.A. Volinsky, Ferrite and austenite phase identification in duplex stainless steel using SPM techniques, Appl. Surf. Sci. 287 (2013) 499–501.
[24] A.F. Ribeiro, L.H. De Almeida, D.S. Dos Santos, D. Fruchart, G.S. Bobrovnitchii, Microstructural modifications induced by hydrogen in a heat resistant steel type HP-45 with Nb and Ti additions, J. Alloys Compd. 356–357 (2003) 693–696, https://doi.org/10.1016/S0925-8388(03)00173-7.

[25] F.C. Nunes, L.H. de Almeida, J. Dille, J.L. Delplancke, I. Le May, Microstructural changes caused by yttrium addition to NbTi-modified centrifugally cast HP-type stainless steels, Mater. Charact. 58 (2007) 132–142.
[26] S. Shi, J.C. Lippold, Microstructure evolution during service exposure of two cast, heat-resisting stainless steels – HP-Nb modified and 20–32Nb, Mater. Charact. 59 (2008) 1029–1040.
[27] R. Voicu, E. Andrieu, D. Poquillon, J. Furtado, J. Lacaze, Microstructure evolution of HP40-Nb alloys during aging under air at 1000°C, Mater. Charact. 60 (2009) 1020–1027, https://doi.org/10.1016/j.matchar.2009.04.007.
[28] R.A. Pedro, Ibañez, G.D. de Almeida Soares, L.H. de Almeida, I. Le May, Effects of Si content on the microstructure of modified-HP austenitic steels, Mater. Charact. 30 (1993) 243–249.
[29] ASTM-A297/A297M, Standard Specification for Castings, Iron-Chromium, Iron-Chromium-Nickel, Corrosion Resistant, for General Application, ASTM International, 2008.
[30] J.E. Stern, B.D. Terris, H.J. Mamin, D. Rugar, Deposition and imaging of localized charge on insulator surfaces using a force microscope, Appl. Phys. Lett. 53 (1988) 2717–2719, https://doi.org/10.1063/1.100162.
[31] M. Nonnenmacher, M.P. O'Boyle, H.K. Wickramasinghe, Kelvin probe force microscopy, Appl. Phys. Lett. 58 (1991) 2921.
[32] K.J. Stevens, A. Parbhu, J. Soltis, D. Stewart, Magnetic force microscopy of a carburized ethylene pyrolysis tube, J. Phys. D Appl. Phys. 36 (2003) 164–168.
[33] K.J. Stevens, A. Parbhu, J. Soltis, Magnetic force microscopy and cross-sectional transmission electron microscopy of carburised surfaces, Curr. Appl. Phys. 4 (2004) 304–307, https://doi.org/10.1016/j.cap.2003.11.034.
[34] I.C. Silva, J.M.A. Rebello, A.C. Bruno, P.J. Jacques, B. Nysten, J. Dille, Structural and magnetic characterization of a carburized cast austenitic steel, Scr. Mater. 59 (2008) 1010–1013.